Removal of *pomt1* in zebrafish leads to loss of α-dystroglycan glycosylation and dystroglycanopathy phenotypes

Brittany F. Karas[#], Kristin R. Terez[#], Namarata Battula, Brian M. Gural, Kyle P. Flannery, Grace Aboussleman, Numa Mubin, M. Chiara Manzini[*]

Department of Neuroscience and Cell Biology, Child Health Institute of New Jersey, Rutgers University-Robert Wood Johnson Medical School, New Brunswick, NJ 08901 USA.

# these authors contributed equally

***Corresponding Author:**

M. Chiara Manzini

Department of Neuroscience and Cell Biology

Child Health Institute of New Jersey

Rutgers University-Robert Wood Johnson Medical School

New Brunswick, NJ 08901 USA

Phone: 732-235-3245

Email: chiara.manzini@rutgers.edu

Abstract

Biallelic mutations in *Protein O-mannosyltransferase 1* (*POMT1*) are among the most common causes of a severe group of congenital muscular dystrophies (CMDs) known as dystroglycanopathies. POMT1 is a glycosyltransferase responsible for the attachment of a functional glycan mediating interactions between the transmembrane glycoprotein dystroglycan and its binding partners in the extracellular matrix (ECM). Disruptions in these cell-ECM interactions lead to multiple developmental defects causing brain and eye malformations in addition to CMD. Removing *Pomt1* in the mouse leads to early embryonic death due to the essential role of dystroglycan in embryo implantation in rodents. Here, we characterized and validated a model of *pomt1* loss of function in the zebrafish showing that developmental defects found in individuals affected by dystroglycanopathies can be recapitulated in the fish. We also discovered that *pomt1* mRNA provided by the mother in the oocyte supports dystroglycan glycosylation during the first few weeks of development. Muscle disease, retinal synapse formation deficits, and axon guidance defects can only be uncovered during the first week post fertilization by generating knock-out embryos from knock-out mothers. Conversely, maternal *pomt1* from heterozygous mothers was sufficient to sustain muscle, eye, and brain development only leading to detectable muscle disease and loss of photoreceptor synapses at 30 days post fertilization. Our findings show that it is important to define the contribution of maternal mRNA while developing zebrafish models of dystroglycanopathies and that offspring generated from heterozygous and knock-out mothers can be used to differentiate the role of dystroglycan glycosylation in tissue formation and maintenance.

42 **Introduction**

43 Dystroglycanopathies are a group of rare autosomal recessive neuromuscular disorders which
44 include the most severe forms of congenital muscular dystrophy (CMD). These diseases also affect the
45 eye and brain and lead to early mortality (1,2). The primary molecular deficit is the loss of interactions
46 between the extracellular portion of the transmembrane glycoprotein dystroglycan, α-dystroglycan (α-
47 DG), and ligands in the extracellular matrix (ECM) (2). These interactions are mediated via a large,
48 specialized O-linked glycan on α-DG termed matriglycan assembled via multiple glycosyltransferases (2,3).
49 Biallelic mutations in *dystroglycan* (*DAG1*, OMIM:128239) itself have been identified as the cause of
50 primary dystroglycanopathy (OMIM:613818, 616538), but they are exceedingly rare (4). Most cases of
51 dystroglycanopathies are deemed secondary and are caused by variants in the glycosyltransferases
52 involved in catalyzing the synthesis of matriglycan (2).

53 *Protein O-mannosyltransferase 1* (*POMT1*, OMIM:607423) catalyzes the addition of an O-linked
54 mannose to α-DG starting the assembly of the functional glycan (5). *POMT1* mutations are one of the
55 most frequent causes of dystroglycanopathy in multiple populations and lead to the full spectrum of
56 disease from limb-girdle muscular dystrophy (POMT1-LGMD, OMIM:609308) to severe CMD disorders
57 affecting the brain and the eyes such as Walker Warburg Syndrome (WWS) (OMIM:236670) (6–8). Global
58 knock-out (KO) of *Pomt1* in the mouse leads to early embryonic lethality similarly to *Dag1* mutants. This
59 is due to the critical role of dystroglycan in Reichert's membrane, a specialized basement membrane in
60 rodent embryos (9,10). Thus, *Pomt1* mouse models have only been studied using conditional approaches
61 (11,12).

62 We sought to develop a novel animal model of dystroglycanopathies by characterizing *pomt1* loss
63 of function in the zebrafish. The zebrafish has become an established model for muscle disease because
64 of the molecular and physiological conservation of disease mechanisms, their external embryonic
65 development, and their fecundity accompanied with small size which allows for high-throughput drug
66 screening for motor phenotypes (13,14). Most zebrafish models for dystroglycanopathies to date have
67 been generated via gene knockdown using morpholino oligonucleotides (MOs) to validate genetic findings
68 in humans. The same array of phenotypes including loss of α-DG glycosylation, shortened body axis,
69 reduced mobility, muscular dystrophy, and eye and brain malformation were found in knockdown models
70 of multiple glycosyltransferases (15–19). However, knockdown approaches are limited by their variable
71 and transient effect. Furthermore, results of *pomt1* knockdown in larvae were unexpectedly mild
72 compared to other dystroglycanopathy zebrafish knockdowns (19).

73 Out of the nineteen dystroglycanopathy genes, there are currently three zebrafish genetic models
74 reported. The *patchytail* mutant was generated via a mutagenesis screen leading to a missense mutation
75 in *dag1* and loss of the protein. These mutants die by 10 days post fertilization and show similar deficits
76 to the morphants, although less severe, which recapitulate multiple aspects of the human presentation
77 in the muscle, eye, and brain (20). KO larvae for the glycosyltransferase *fukutin-related protein* (*fkrp*) more
78 closely phenocopied the morphants and were then used to study the effects of overexpression of the
79 most common *FKRP* (OMIM: 606596) missense variant leading to *FKRP*-related LGMD (OMIM:607155) to
80 identify compounds that could ameliorate motor phenotypes by drug screening (21). Interestingly, no
81 motor or developmental phenotypes were described for zebrafish CRISPR mutants developed for another
82 glycosyltransferase *protein O-mannose β-1,2-N-acetylglucosaminyltransferase* (*pomgnt1*) (22). However,
83 *pomgnt1* KOs showed photoreceptor degeneration in the retina between 2 and 6 months of age,
84 reflecting retinal deficits identified in patients (23). Hypomorphic variants in *POMGNT1* have also been
85 linked with non-syndromic retinitis pigmentosa (24). These studies indicated that relevant phenotypes
86 resulting from global KOs of dystroglycanopathy genes can be successfully modeled in zebrafish. Due to
87 the genetic heterogeneity of dystroglycanopathies, testing zebrafish models for multiple genes will be
88 beneficial to identify compounds that would be effective in individuals with distinct genetic causes.
89 Here, we show that *pomt1* KO zebrafish show varying degree of muscle, eye, and brain
90 phenotypes depending on whether *pomt1* mRNA is provided to the oocyte from the mother. Since the
91 eggs are externally fertilized, zebrafish females provide nutrients, mRNAs, and proteins to support early
92 development in the yolk (25). *pomt1* KOs obtained from heterozygous mothers can compensate for the
93 early developmental phenotypes by having maternally provided Pomt1 glycosylate α-DG. More severe
94 phenotypes appear when KO embryos are generated by a KO mother. Our work indicates that special
95 consideration must be taken regarding the potential maternal contribution in future dystroglycanopathy
96 mutants.
97
98 **Results**
99 *A late nonsense allele in pomt1 leads to complete protein loss and loss of α-DG glycosylation*
100 In order to determine whether loss of *pomt1* would lead to dystroglycanopathy phenotypes in
101 the zebrafish, we obtained a *pomt1* line generated through a N-ethyl-N-nitrosurea (ENU) mutagenesis
102 screen by the Zebrafish Mutation Project (ZMP line: sa146678, kind gift of Dr. James Dowling, Sick Kids,
103 Toronto, Canada) (**Fig.1A**) (26). This line introduced a variant in exon 19 of *pomt1* (NM_001048067:
104 c.1911T>A) leading to a stop codon (NP_001041532: p.Tyr637Ter) towards the C-terminus of the 720

amino acid protein. Since multiple homozygous nonsense and frameshift variants had been reported in humans to cause the most severe form of dystroglycanopathy, WWS (27,28), we hypothesized that this zebrafish variant could lead to nonsense mediated decay of the mRNA and complete protein loss. We bred the p.Tyr637Ter variant into homozygosity and confirmed the variant by Sanger sequencing (**Fig.1B**). Through quantitative PCR (qPCR) analysis we found that *pomt1* mRNA was reduced in both heterozygous and homozygous fish between 5 and 40 days post fertilization (dpf) with the exception of the 10 dpf timepoint where there was an increase (**Fig.1C**). The Pomt1 protein was completely lost at 30 dpf in homozygous animals and no additional truncated band was noted, apart from a non-specific band which is also present in wild-type (WT) samples (**Fig.1D**). In parallel, we confirmed that Pomt1 function was completely lost. No α-DG glycosylation was found using a glyco-specific antibody in wheat germ agglutinin (WGA) enriched zebrafish head tissue from 30 dpf animals, though β-DG expression was preserved (**Fig.1E**). In summary, the *pomt1*^{Y637X} line leads to complete loss of function of Pomt1 and will be termed as *pomt1* KO.

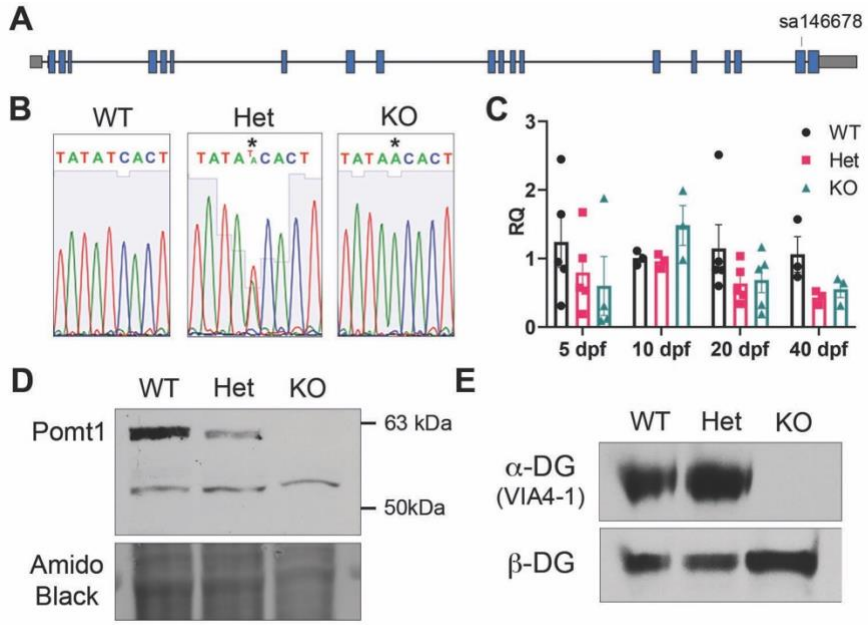

Figure 1. *pomt1* nonsense variant leads to complete loss of protein and protein function. A. Schematic of the gene structure of *pomt1* including the location of the variant in exon 19. **B.** Sanger sequencing validation shows the stop codon generated in the KO genome. **C.** qPCR analysis showed consistent reduction in *pomt1* mRNA apart from 10 dpf. **D.** Pomt1 is completely absent on Western blot in 30 dpf protein lysates. **E.** α-DG glycosylation is absent in KO tissue while β-DG expression is preserved.

Loss of pomt1 from heterozygous crosses leads to reduced survival and muscle disease

No phenotypes had been reported in *pomt1* KO zebrafish larvae by the ZMP. Thus, we performed a comprehensive analysis of *pomt1* KO fish obtained from heterozygous (Het) parents. Survival analysis revealed that *pomt1* KO juveniles start dying between 30 dpf and 40 dpf (30 dpf: WT 24.3±8.0%, n=18; Het 49.0±9.5%, n=41; KO 27.7±2.0%, n=17, N=3 clutches. 40 dpf: WT 28.0±4.0%, n=22, Het 60.3±7.5%, n=46, KO 11.7±3.5%, n=11, N=3 clutches) with no survival observed beyond 70 dpf (**Fig.2A**). While no morphological differences were noted at 5 and 20 dpf, significant differences in body length emerged at 30 dpf (WT 8.5±0.5 mm, n=18; Het 7.3±0.3 mm, n=41; KO 6.2±0.2 mm, n=17; WT-Het p=0.039 *, WT-KO p=0.0005 ***) (**Fig. 2B**). *pomt1* KO juveniles were smaller and showed a delay in development with less prominent dorsal and anal fins (**Fig.2C**). Interestingly, the surviving KO fish at 40 dpf were the largest of that genotype (WT 9.6±0.4 mm, n=22; Het 9.9±0.3 mm, n=46; KO 8.5±0.4 mm, n=11). This finding suggests that smaller KO fish likely died due to the inability to compete for food. As such, only the least affected fish survived.

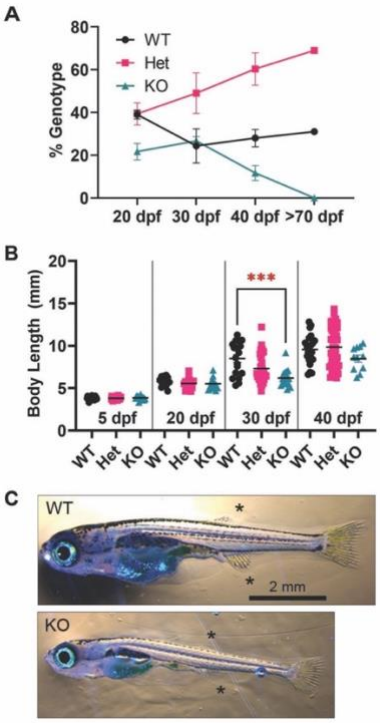

Figure 2. *pomt1* KO fish show reduced survival and size. A. Survival curves show a drop in *pomt1* KO juveniles after 30 dpf. **B.** Significant size differences are evident in KO fish at 30 dpf, but not in the surviving KO fish at 40 dpf. *** p<0.001 **C.** *pomt1* KO fish at 30 dpf appear underdeveloped with less prominent dorsal and anal fins (asterisks). Scale bar: 2mm.

143 We tested motor function in an automated DanioVision™ tracking system where the fish were
144 allowed to swim freely for 30 minutes. No differences were noted in 5 dpf larvae (**Suppl. Fig. 1A-C**).
145 While only a trend for reduced distance covered and swimming velocity was found in 30 dpf *pomt1* KOs
146 (WT n=15, Het n=37, KO n=13, N=3 clutches. Distance: WT 870.5±84.9 cm, Het 803.9±54.7 cm, KO
147 666.2±88.9 cm, WT-KO p=0.51. Velocity: WT 0.485±0.047 cm/s, Het 0.449±0.030 cm/s, KO 0.380±0.051
148 cm/s, WT-KO p=0.62) (**Fig.3A-B**), we found a significant reduction in acceleration when compared to
149 both Het and WT fish (WT 420.1± 24.0 cm/s^2, Het 401.6±23.3 cm/s^2, KO 291.0±27.8 cm/s^2, WT-KO
150 p=0.024 *, Het-KO p=0.018 *) (**Fig. 3C**). Histological analysis of the muscle at 30 dpf was complicated by
151 the extreme fragility of the tissue in KO animals where myofibers tended to fragment. Via hematoxylin-
152 eosin staining in paraffin sections, we found that myofibers where short and separated from each other
153 often with gaps in the myosepta (**Fig.3D**). In immunohistochemistry on cryosections, we showed that
154 Pomt1 localizes in both longitudinal and junctional sarcoplasmic reticulum (SR), as previously described
155 in mouse and humans (29), and that ryanodine receptor 1 (Ryr1) in the SR around the T tubules is
156 greatly reduced as found in *patchytail,* the *dag1* mutant fish (**Fig.3E**) (20). The same loss of Ryr1 staining
157 was also present at 10 dpf, when no other phenotypes were evident (**Suppl. Fig.1D**). Although milder
158 than expected, these results show overall that loss of *pomt1* in the zebrafish leads to deficits in muscle
159 function and structure.

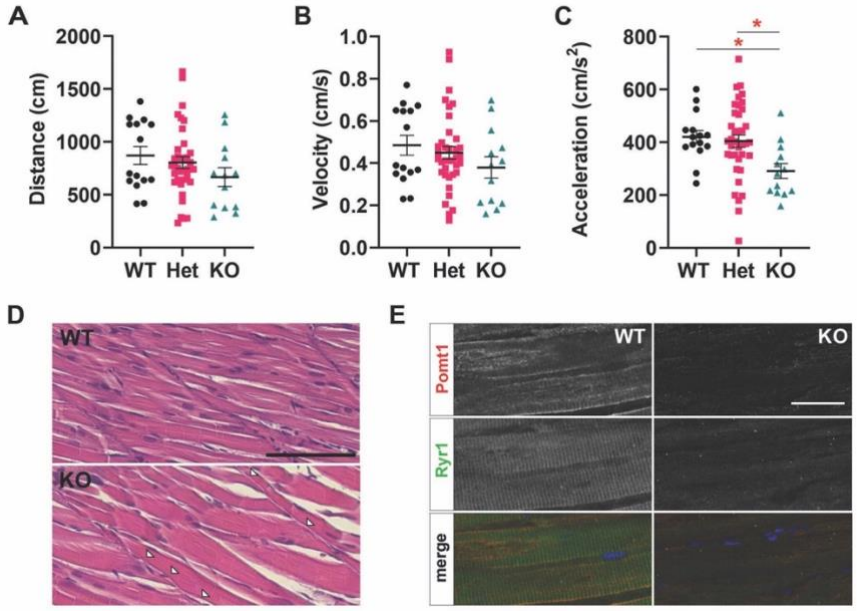

160

161 **Figure 3. Muscle phenotypes in 30 dpf *pomt1* KO juvenile zebrafish. A-C.** Automated tracking of motor
162 activity showed only a trend for reduction in distance (**A**) and velocity (**B**), but significant reduction in
163 acceleration (**C**) in KO animals compared to WT and Het. * p<0.05 **D.** Muscle histology in paraffin

164 sections stained with hematoxylin and eosin showed separated fibers of variable size and gaps in the
165 myosepta (arrowheads). Scale bar: 50 μm. **E.** Muscle immunohistochemistry on cryosections showed
166 loss of Pomt1 staining. Ryr1 from the junctional SR around T tubules is also absent in KO muscle. Scale
167 bar: 20 μm.
168
169 *pomt1 loss-of-function disrupts photoreceptor synapses*
170 While the brain of 30 dpf *pomt1* KO fish showed no major structural abnormalities, a mutant for
171 the glycosyltransferase *pomgnt1* showed photoreceptor degeneration between 2 and 6 months of age
172 (22). While eye size in *pomt1* KOs was highly variable and only trended towards being smaller, it was
173 proportional to body size (**Suppl. Fig.2A**). We chose to analyze the smaller *pomt1* KO fish that were likely
174 to be more severely affected. Retinal thickness and photoreceptor layer thickness were reduced at 30
175 dpf and the photoreceptor layer was disproportionally thinner than the retina (**Suppl. Fig.2B**.
176 Retina/photoreceptor ratio. WT n=6: 0.390±0.018, KO n=5: 0.297±0.027, p=0.015 *)**.** Through
177 immunohistochemical analysis we noted several disruptions in the photoreceptor layer and in the outer
178 plexiform layer (OPL) where photoreceptor pedicles form synapses with bipolar cells and horizontal cells
179 to begin the transmission of light signals. Immunostaining with the red/green double cone maker
180 arrestin3a (Arr3a) which also accumulates at the presynaptic pedicles of the photoreceptors (30)
181 showed a disruption in the organization of terminals in the OPL with some terminals retracting among
182 the photoreceptor nuclei (**Fig.4A**). Expression of Gnat2, a cone-specific α-transducin subunit necessary
183 for the phototransduction cascade and color vision (31), showed reduced staining in the outer limiting
184 membrane and in the photoreceptor outer segments (**Fig.4A**). In addition, the rod and green cone
185 marker, zpr-3, which is predicted to bind outer segment opsins (32) also showed localized reduced
186 staining, though rod outer segments appear present in autofluorescence (**Fig.4B**). OPL disorganization
187 was evident in the Hoechst nuclear staining, where localized misalignments of photoreceptor nuclei
188 were present, as well as smaller and misshapen horizontal cell nuclei (**Fig.4B**). These disruptions
189 suggested a loss of photoreceptor-bipolar cell synapses. Discontinuities in the expression of presynaptic
190 protein synaptophysin (Syp) were present wherever photoreceptor pedicles were lost (**Fig.4C**). Overall,
191 our results were similar to the phenotypes in both *pomgnt1* KO zebrafish and *Pomt1* conditional
192 removal in photoreceptors in mice where loss of dystroglycan glycosylation leads to disruptions at
193 photoreceptor ribbon synapses and subsequent photoreceptor degeneration (12,22).
194

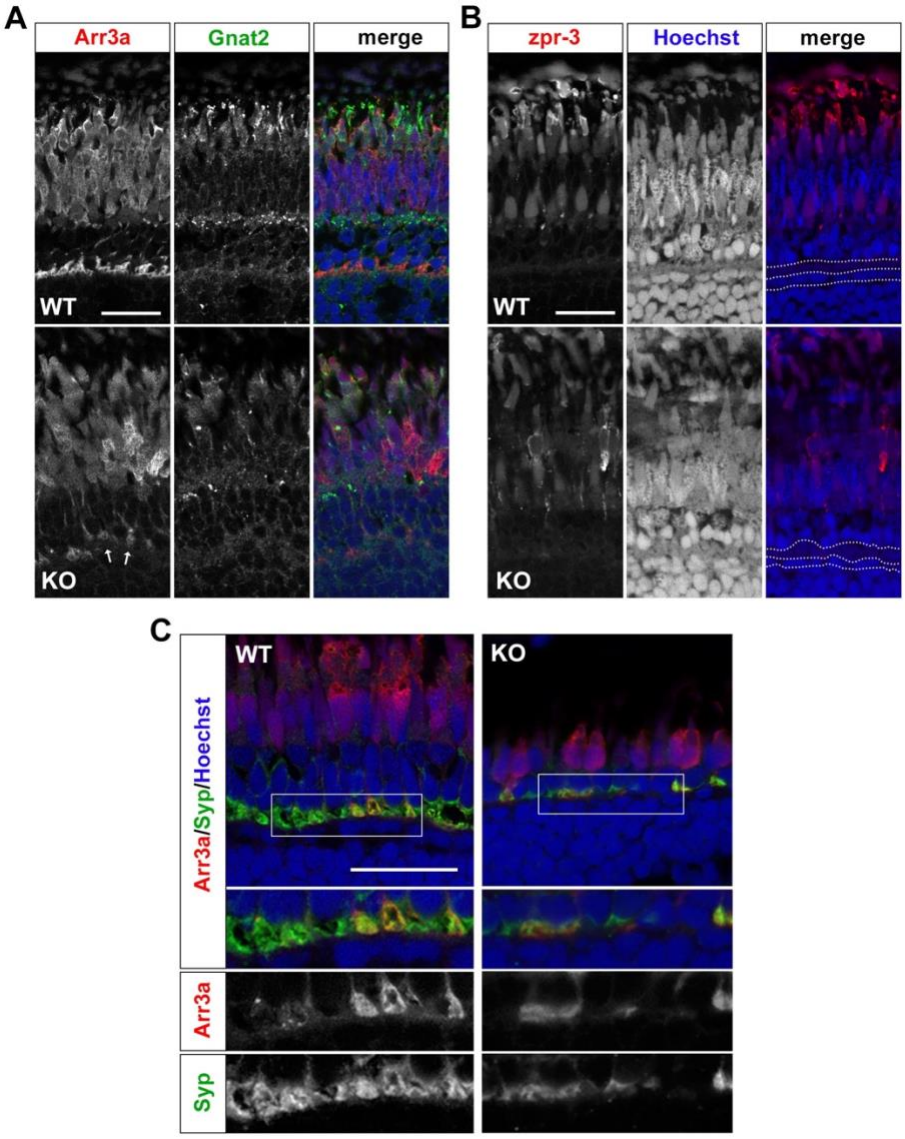

Figure 4. Photoreceptor synapses are disrupted in *pomt1* KO retinae. A. Red/green double cone marker arrestin 3a (Arr3a) shows both a disorganization in the outer segment and retraction of photoreceptors pedicles in the outer plexiform layer (OPL) (arrows). Cone-specific α-transducin (Gnat2) staining is also reduced and lost in the outer limiting membrane. Scale bar: 20 μm **B.** zpr-3 staining is reduced, but rods appear present in autofluorescence. Nuclear staining with Hoechst shows disorganization in the OPL and disruption in the nuclei of the horizontal cells below the OPL. OPL and horizontal cell nuclear layer are outlined by the white dotted lines. Scale bar: 20 μm **C.** Synaptophisin (Syp) staining is discontinuous and showing loss of synaptic contacts. The white boxes outline the inset where immunostaining for each antibody is shown below. Scale bar: 20 μm

206 *More severe dystroglycanopathy phenotypes are present when pomt1 is removed from fertilized oocytes.*

207 Even though muscle and eye phenotypes characteristic of dystroglycanopathies were present in
208 the *pomt1* KO juveniles, they presented later than expected when compared to *dag1* zebrafish mutants
209 (20). Not only are zebrafish notorious for being able to compensate for genetic mutations (33), but also
210 display a fundamental difference from mammals in that a deposit of mRNA and proteins provided by the
211 mother in the yolk sac supports early development of the externally fertilized egg (25). *pomt1* mRNA is
212 highly expressed in the maternal deposit (19) and glycosylated α-DG is stable for several days in tissues
213 (34). We hypothesized that the appearance of dystroglycanopathy phenotypes in *pomt1* KO fish was
214 delayed due to residual Pomt1 function in the embryo provided by the Het mother.

215 Molecular investigation by western blot at 5 dpf indicated that *pomt1* KO larvae obtained from
216 Het females (herein KO^{Het}) retained both the Pomt1 protein and substantial α-DG glycosylation (**Fig.5A**).
217 We were able to support several KO^{Het} females to survive to breeding age by reducing stocking density
218 and decreasing competition for food. This allowed us to investigate whether offspring from oocytes
219 lacking *pomt1* would have more severe phenotypes. 5 dpf *pomt1* KO larvae obtained from KO female x
220 Het male crosses (KO^{KO}) showed no residual Pomt1 expression or α-DG glycosylation (**Fig.5B**). As
221 observed in the *dag1* mutant zebrafish (20), survival in *pomt1* KO^{KO} larvae decreased rapidly after 10 dpf
222 (**Fig.5C**). In parallel, body size was significantly reduced starting at 10 dpf (Het: 4.39±0.05 mm, n=51;
223 KO^{KO}: 3.97±0.05 mm, n=43, N=3 clutches. p<0.0001 ***) (**Fig.5D**). Interestingly, size disparities were
224 variable at 20 dpf, the timepoint at which KO^{KO} fish started dying. Clutches where most KO^{KO} larvae had
225 died showed no significant size differences (Het: 5.63±0.10 mm, n=63; KO^{KO}: 5.40±0.20 mm, n=12, N=3
226 clutches. p=0.366) (**Suppl. Fig.3A**), while a clutch with a 50/50 ratio of Hets and KO^{KO}s showed a
227 significant size reduction (Het: 5.93±0.14 mm, N=1, n=12; KO^{KO}: 5.08±0.11, N=1, n=12. p<0.0001 ***)
228 (**Fig. 5D, Suppl. Fig.3B**), again showing that the largest fish can survive better. By 30 dpf, the few
229 surviving fish were smaller than the Het^{KO} siblings (Het: 7.17±0.14 mm, n=58; KO^{KO}: 6.22±0.20, n=8, N=3
230 clutches. p<0.0001 ***).

231 Locomotor activity was significantly impacted in pomt1 KO^{KO} larvae at 5 dpf with reductions in
232 distance traveled, velocity and acceleration, showing that even if survival and size were not affected
233 mobility was already severely impacted at an early age (Het n=57, KO^{KO} n=36, N=3 clutches. Distance:
234 Het: 345.2±117.3 cm, KO^{KO}: 231.4±0.11, p<0.0001 ***; Velocity: Het: 0.19±0.06 cm/s, KO^{KO}: 0.13±0.04
235 cm/s, p<0.0001 ***; Acceleration: Het: 166.6±67.6 cm/s^2, KO^{KO}: 81.63±67.34 cm/s^2, p<0.0001
236 ***)(**Fig.6A-C**). Muscle integrity analysis using birefringence using polarized light to detect muscle fiber
237 organization showed reduced intensity (**Fig.6D**). Immunohistochemistry on cryosections using

238 fluorescently stained phalloidin to outline actin in muscle fibers showed some modest discontinuities in
239 staining and revealed widenings in the myosepta as observed at 30 dpf in KO^{Het}s indicating the beginning
240 of muscle disease (**Fig.6E**).
241

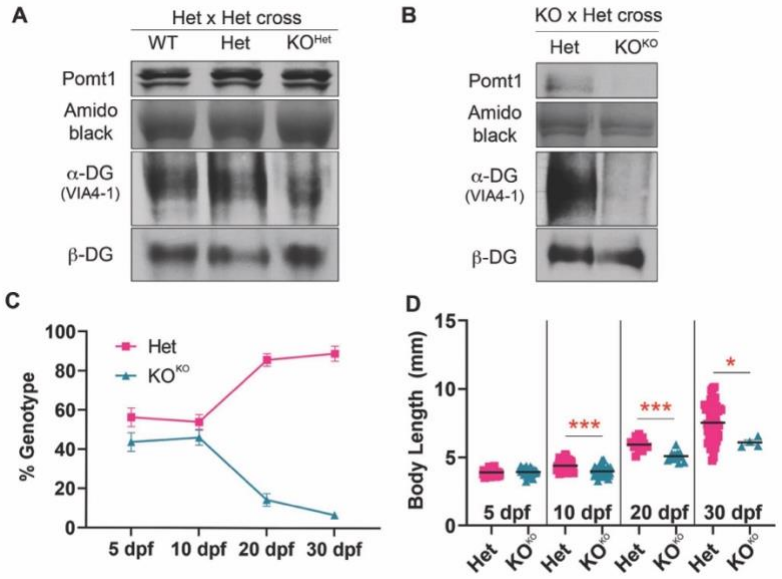

242
243 **Figure 5. Removal of maternal *pomt1* mRNA contribution from oocytes leads to earlier phenotypes in**
244 ***pomt1* KO^{KO} larvae. A.** Residual Pomt1 is present in 5 dpf KO^{Het} larvae derived from Het X Het crosses, as
245 is α-DG glycosylation. **B.** Both Pomt1 and α-DG glycosylation are absent at 5 dpf in KO^{KO} larvae obtained
246 from KO mothers crossed with Het fathers. **C.** Survival in *pomt1* KO^{KO} zebrafish is reduced starting at 10
247 dpf. **D.** Reduced body size is observed in KO^{KO} larvae and juveniles starting at 10 dpf. *** $p<0.001$, *
248 $p<0.05$
249
250 **Figure 6 (image on following page). *pomt1* KO^{KO} larvae show reduced mobility and muscle disease at 5**
251 **dpf. A-C.** A significant reduction in total distance traveled (**A**.), velocity (**B.**) and acceleration (**C.**) are
252 found in *pomt1* KO^{KO} larvae upon automated mobility analysis when compared to Het siblings. ***
253 $p<0.001$. **D.** Birefringence analysis showed patchy light diffraction through the KO^{KO} muscle showed
254 disorganized muscle tissue. Scale bar: 500 μm. **E.** Staining with fluorescently labeled phalloidin to
255 visualize actin in muscle fibers revealed some fiber disorganization, variable staining intensity, and
256 increased space between muscle segments in the myosepta (arrowheads) of KO^{KO} larvae. Scale bar: 100
257 μm

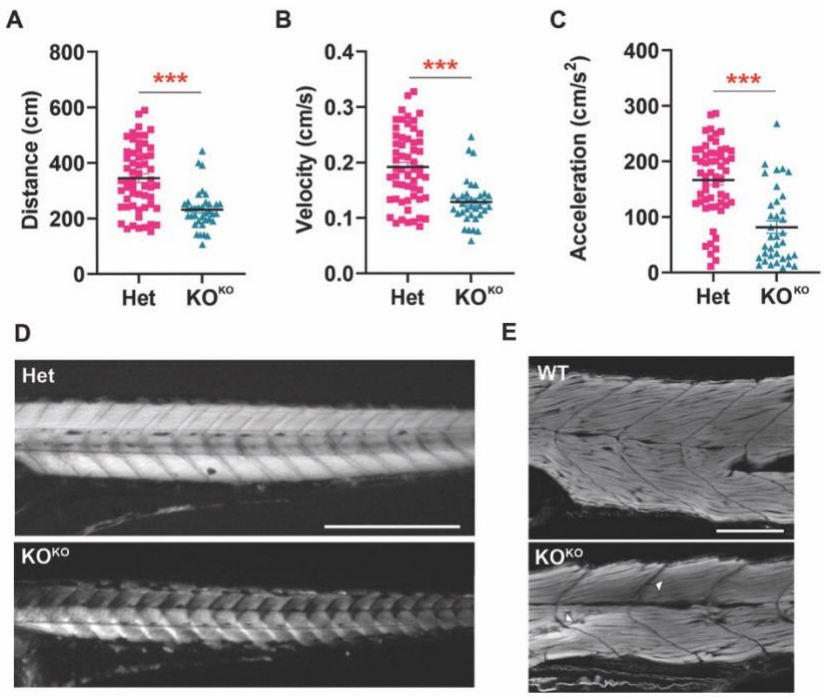

258

259

260 Retinal phenotypes observed at 30 dpf in KO^{Het} fish were present at 5 dpf in the KO^{KO} larvae.
261 Arr3a staining in cone photoreceptors was patchy and nuclei were disorganized in the outer nuclear
262 layer of photoreceptors (**Fig.7A**). Synaptic staining with Syp in the OPL was discontinuous, often
263 extending into the outer nuclear layer indicating retraction of photoreceptor pedicles indicating an early
264 loss of synapses between photoreceptors and bipolar cells (**Fig.7A**, **Suppl. Fig.4**). One major phenotype
265 caused by loss of α-DG glycosylation in mice is the disruption of axonal tracts in the brain caused by loss
266 of interaction with axon guidance cues (35,36). One example is the disruption in retinal ganglion cell
267 sorting and fasciculation in the optic nerve which is controlled by binding to the midline crossing cue
268 Slit2, an α-DG ligand (36,37). We did not see any deficits in axonal crossing and fasciculation in the optic
269 chiasm of 30 dpf KO^{Het} fish (**Suppl. Fig.5**), but we wondered whether the maternal deposit of *pomt1* was
270 sufficient to bypass this early developmental phenotype. When we analyzed the optic chiasm using the
271 zn8 antibody that labels retinal ganglion cells and their axons, we noted substantial axonal
272 defasciculation following axon crossing at the optic chiasm of KO^{KO} larvae reminiscent of phenotypes
273 found following *slit2* knockout and knockdown in the fish (**Fig.7B**) (38). Thus, *pomt1* loss of function
274 early in development in the zebrafish also recapitulates some of the central nervous system phenotypes
275 found in higher vertebrates.

276

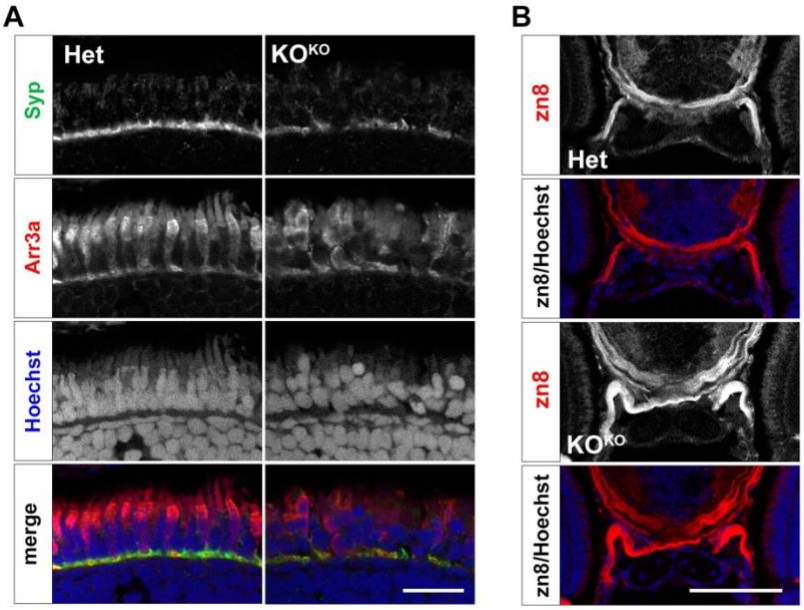

Figure 7. Retinal and axon guidance phenotypes are found at 5 dpf in *pomt1* KO^{KO} larvae. A. Discontinuities in synaptophysin (Syp) staining are found in the outer plexiform layer (OPL) of *pomt1* KO^{KO} retinae. Red/green double cone marker arrestin 3a (Arr3a) again shows disorganized outer segments and patchy staining and altered shape of photoreceptors pedicles. Nuclear staining with Hoechst shows disorganization disruption in the photoreceptor nuclei and in horizontal cell nuclei below the OPL. Scale bar: 20 μm. **B.** Visualization of the optic nerve using the zn8 antibody that labels retinal ganglion cell axons shows axon defasciculation after optic chiasm crossing. Scale bar: 50 μm.

Discussion

Here, we showed that *pomt1* KO zebrafish can be used to model dystroglycanopathy phenotypes in the muscle, eye, and brain with variable severity. For our initial analysis of this mutant strain we focused on phenotypes identified in other dystroglycanopathy models in fish and mouse. The phenotypes found in *pomt1* KO^{Het} obtained from heterozygous crosses were milder than those observed in the *dag1* loss of function fish (20) suggesting that compensation may be present. We found that this was due to high *pomt1* mRNA expression in the maternal deposit in the oocyte supporting α-DG glycosylation during the first week post fertilization. While we still found Pomt1 expression at 5 dpf in KO^{Het} larvae, the protein was largely absent from the muscle at 10 dpf. In parallel, *pomt1* mRNA levels that were consistently lower than WT at all other timepoints were increased at 10 dpf likely in response to loss of the maternal protein. Even if Pomt1 was lost by 10 days, studies in mouse muscle have shown that dystroglycan can remain for up to 20 days in tissues (39). We found that in *pomt1* KO^{Het} fish α-DG glycosylation was completely lost by

298 30 dpf when disease-related phenotypes in the muscle and retina began to emerge. KO^{Het} juveniles
299 maintained at high stocking density started dying at 30 dpf with no survivors found past 70 days. We noted
300 that *pomt1* KOs surviving the longest were the largest and showed the least severe phenotypes suggesting
301 that impaired mobility and/or vision may prevent the smaller KOs from having access to food in the tank.
302 Some KO fish could only be raised when stocking density was reduced to remove competition for food.
303 These results indicate that even when the early developmental roles of α-DG are conserved, continued
304 Pomt1 expression is necessary to maintain muscle function and retinal photoreceptors integrity.

305 By raising KO females, we were able to obtain oocytes completely devoid of *pomt1* mRNA to
306 generate true developmental KOs where α-DG O-mannosylation is prevented from time of fertilization.
307 *pomt1* KO^{KO}s closely resembled other dystroglycanopathy models in both zebrafish and mouse. As in the
308 *dag1* mutant, *patchytail*, *pomt1* KO^{KO}s died within the first 2 weeks post fertilization. The muscle displayed
309 abnormal birefringence, openings in the myotendenous junctions or myosepta between muscle
310 segments, and loss of Ryr1 staining in the SR. These deficits led to substantial mobility phenotypes at 5
311 dpf. At the same time, we identified defects in photoreceptor synapses and optic nerve fasciculation in
312 the KO^{KO} larvae reflecting loss of α-DG ligand binding necessary for synapse formation and axon guidance
313 that had been previously described in *pomt1* conditional mouse models and *pomgnt1* mutant zebrafish
314 (12,22).

315 α-DG can bind to a variety of proteins containing laminin-G domains (40) and several of its ligands
316 have important roles in axon guidance and synapse formation in the brain and peripheral nervous system
317 (35,37,41). Slits are involved in guiding axons in crossing the midline of the body and contribute to the
318 formation of the optic chiasm where axons from each eye target brain regions on the opposite side (42).
319 α-DG was shown to bind to the laminin-G domain of Slit2 to organize axonal crossing (37) and the
320 phenotypes observed in the *pomt1* KO^{KO} larval optic chiasm are similar to the enlarged and disorganized
321 axonal tract found in *slit2* KO zebrafish (43). Another α-DG ligand is pikachurin, a postsynaptic adhesion
322 protein involved in the formation and maintenance of photoreceptor ribbon synapses (41,44). Ribbon
323 synapses are highly specialized structures in the photoreceptor pedicles in the OPL mediating rapid
324 transmission of visual signals to the dendrite tips of horizontal cells and bipolar cells. When the bond
325 between α-DG and pikachurin is lost, the synapse comes apart and photoreceptors pedicles retract
326 eventually leading to photoreceptor degeneration and loss of vision (12,41,44). Our findings in *pomt1*
327 KO^{KO}s closely recapitulate phenotypes in a mutant mouse line where *Pomt1* is conditionally removed in
328 photoreceptors (12). Additional analyses will be needed to determine whether synapses and laminar
329 organization in other retinal layers are also affected as described in mouse models (45). Changes in

330 synaptophysin staining in the inner plexiform layer shown in our supplementary data suggest that this
331 may be the case. Overall, early developmental phenotypes caused by loss of matriglycan binding in
332 multiple tissues are present in the *pomt1* KO^{KO} supporting the need to further study of this model to
333 determine the impact of these mutations in the brain and peripheral nervous system.

334 While *pomt1* KO^{KO} and the *dag1* ENU mutant are similar, their phenotypes are overall less severe
335 than those observed the *fkrp* mutant line which in turn recapitulate morphant models for *fkrp* and other
336 glycosyltransferases mutated in dystroglycanopathies (16,17,21,46). Morphants for *fkrp*, *pomgnt1* and
337 *b3galnt2* larvae show early mortality, shorter body, smaller head and eyes and severe cardiac edema. On
338 the other hand, *pomt1* morphants were less severe than other morphants showing milder morphological
339 disruptions (19). Thus, we believe that KO^{KO} animals reflect complete loss of function of *pomt1* in the fish
340 and can be studied as a valid model of dystroglycanopathy phenotypes in the muscle, eye, and brain. Our
341 study stresses how maternal mRNA and protein contribution must be taken into consideration when
342 generating dystroglycanopathy models since the long-lasting presence of glycosylated α-DG can mask
343 developmental phenotypes in the embryo. At the same time, a later onset model where pathogenesis
344 progresses more slowly like the *pomt1* KO^{Het} fish could still be used to study the involvement of α-DG
345 glycosylation in maintenance of tissue function. Both versions of this zebrafish model could be used to
346 investigate therapeutic interventions in multiple tissues at different stages and severity of disease.
347

348 **Materials and Methods**

349 *Zebrafish Husbandry*

350 All experiments and procedures were conducted according to institutional guidance and approved by
351 the Rutgers University Institutional Animal Care and Use Committee. *pomt1* mutant line was a kind gift
352 from James Dowling (Sick Kids, Toronto, Canada). These animals were generated from the Zebrafish
353 Mutation Project (line: sa146678, ZFIN ID: ZDB-ALT-130411-3355) on an AB background (26). The
354 breeding stocks were bred and housed in recirculating Tecniplast USA systems under a 14/10 h
355 light/dark (LD) cycle at 28°C and fed twice daily. To produce embryos, male and female zebrafish were
356 paired in the evening, and spawning occurred within 1 h of lights-on the following morning. Embryos
357 were placed in 10 cm petri dishes with egg water containing methylene blue (5×10^{-5} % w/v) and raised
358 under LD cycles at 28°C.
359

360 *Genotyping*

361 DNA from larval tails and juvenile and adult tail fins was extracted using the Extract-N-Amp Tissue PCR
362 Kit (Millipore Sigma). After verifying SNP location with Sanger sequencing at Azenta Life Sciences,
363 genotype was determined using a Custom TaqMan SNP Genotyping Assay (Assay ID: ANRWEV2, Thermo
364 Fisher).
365
366 *Quantitative Real-Time PCR (qPCR) Gene Expression Analysis*
367 Total RNA was isolated from embryo composite samples or adult tissue using ReliaPrep RNA Tissue
368 Miniprep System (Promega). Reverse transcription was performed on RNA to produce cDNA for RT-PCR
369 using an iScript Reverse Transcription Supermix (Bio-Rad) using a Bio-Rad T100 Thermal Cycler. RT-PCR
370 reactions were performed in triplicate using PowerUp SYBR Green Master Mix (Thermo Fisher). cDNA
371 amplification was performed for 40 cycles on a QuantStudio 3 (Applied Biosystems) and recorded with
372 QuantStudio Design and Analysis Software. Analysis was conducted as $\Delta\Delta$CT using *elf1-alpha* or *rpl13* as
373 an endogenous control. All primer sequences are available upon request.
374
375 *Wheat Germ Agglutinin Enrichment and Western Blot Analysis*
376 Total zebrafish protein was extracted from composite samples (5 dpf; N=60 and 30 dpf; N=3) using lysis
377 buffer (50 mM Tris pH 8, 100 mM NaCl, 1 mM PMSF, 1 mM Na Orthovanadate, 1% Triton-X 100)
378 containing protease inhibitor cocktail (Millipore Sigma), and 3 rounds of hand homogenization and
379 vortexing. Samples were then sonicated in a Bransonic B200 Ultrasonic Cleaner (Millipore Sigma) 3 times
380 for 5 minutes. Next samples were spun down at 4°C for 20 minutes at 15,000 xg. The supernatant was
381 collected from the samples and sonicated once for 5 minutes. Total protein concentration was
382 determined using a BCA Protein Assay kit (G-Biosciences) and subsequently treated with DNase I (New
383 England Biolabs). 400-500 μg of protein was then added to 50 μl of Wheat Germ Agglutinin (WGA)
384 agarose bound beads (Vector Laboratories) filled to a volume of 300 μl with Lectin Binding Buffer (20
385 mM Tris pH 8, 1 mM $MnCl_2$ and 1 mM $CaCl_2$) in a 1.5 ml tube and rocked overnight at 4°C. Samples were
386 centrifuged at 15,000 xg for 2 minutes and the supernatant was collected. Volumes of supernatant
387 containing 60 μg of protein were set aside for detection of Pomt1. Glycoproteins were eluted by boiling
388 at 100°C for 10 minutes using 4x Laemmli sample buffer (Bio-Rad). Proteins were separated using a 4-
389 12% Bis-Tris Protein SDS-PAGE Gel (Life Technologies). Samples were transferred to a nitrocellulose
390 membrane (Thermo Fisher) and stained with 0.1% naphthol blue black (amido black) (Millipore Sigma)
391 to detect protein transfer and for total protein quantification. The membranes were blocked for 1 hour
392 with 5% milk in Tris-Buffered Saline with 0.1% Tween (TBST) and subsequently probed with 1:100 anti-α-

393 Dystroglycan antibody, clone VIA4-1 (05-298, Millipore Sigma) and 1:1,000 anti-β-Dystroglycan antibody
394 (ab62373, Abcam) or anti-POMT1 (A10281, ABclonal) overnight at 4°C. Then probed with 1:3,000
395 peroxidase AffiniPure donkey anti-mouse IgG and 1:20,000 peroxidase AffiniPure donkey anti-rabbit IgG
396 (Jackson ImmunoResearch). After washing with TBST, the blots were developed using
397 chemiluminescence Pierce ECL Western Blotting Substrate on CL-XPosure™ Film (Thermo Fisher).
398
399 *Morphological Analysis*
400 Larvae and juvenile zebrafish were anesthetized in 0.016% w/v tricaine methane sulfonate (Tricaine,
401 MS-222) and immobilized in 5% methyl cellulose for imaging with a M165 FC stereo microscope and LAS
402 Software V4.21 (Leica Microsystems). Total body length measurements and eye area were quantified
403 using Fiji/ImageJ software (47). Retinal and photoreceptor layer thickness were measured on
404 cryosections prepared as described below and stained with Hoechst 33342 (1:10,000, Thermo Fisher)
405 also using Fiji/ImageJ.
406
407 *Automated Mobility Tracking*
408 Automated mobility assays were conducted by randomizing 5, 20, and 30 dpf zebrafish into sterile 96
409 and 24-well plates filled with 200 μl and 2 ml of system water, respectively. Fish were then habituated in
410 the DanioVision™ Observation Chamber (Noldus Information Technology, Wageningen) for 30 minutes
411 at a controlled temperature of 28°C. Locomotor activity was tracked for 30 minutes using EthoVision® XT
412 video tracking software. A minimum of three unique breeding sets were used to compile results at each
413 timepoint.
414
415 *Fluorescent Immunohistochemisty*
416 Zebrafish larvae at 5 dpf were euthanized with tricaine and a small portion of the tail was cut to use for
417 genotyping. The remaining fish body was fixed in 4% paraformaldehyde overnight at 4°C. Larvae were
418 washed three times in 1x PBS, then cryoprotected in 15% sucrose with 0.025% sodium azide followed by
419 30% sucrose with 0.025% sodium azide. Larvae were embedded in Tissue Freeze Medium (TFM) (General
420 Data Healthcare) and frozen in 2-methyl butane with dry ice. Juvenile fish processing required the addition
421 of a decalcification step in Cal-Ex (Fisher Scientific) following fixation for 1 hour and 15 minutes rocking at
422 4°C. Cryosections were performed using a Leica CM1850 UV Cryostat (Leica Microsystems) at 10 µm for 5
423 dpf, 12 µm for 10 dpf, and 16 µm for 30 dpf. Primary antibodies were applied overnight at 4°C in 1%
424 normal goat serum (NGS) with 0.1% Triton following a blocking step with 10% NGS. Secondary

425 immunostaining was applied for 1 hour. The following antibodies were used: primary - POMT1 (A10281,
426 1:100, ABclonal), Gnat2 (A10352, 1:200, ABclonal), Synaptophysin (ab32127, 1:100, Abcam), Ryr1 (MA3-
427 925, 1:100, Thermo Fisher), zpr-1 (Arr3a) (zpr-1, 1:200, ZIRC), zpr-3 (zpr-3, 1:200, ZIRC), zn-8 (zn-8-s, 1:100,
428 DSHB); secondary - goat anti-mouse IgG Alexa Fluor 568, goat anti-rabbit Alexa Fluor 488 or goat anti-
429 rabbit Alexa Fluor 568 (all from Thermo Fisher). Slides were washed twice in 1x PBS at room temperature
430 and Hoechst 33342 (1:10,000, Thermo Fisher) was applied in 1x PBS for 5 minutes. F-actin/phalloidin
431 staining was performed using Acti-Stain™ 555 (Cytoskeleton Inc.) at a concentration of 100 nM in 1x PBS
432 and kept in the dark for 30 minutes at room temperature. Slides were then washed three times in 1x PBS
433 for 2 minutes. Slides were coverslipped using ProLong™ Gold Antifade Mountant (Thermo Fisher). Images
434 were taken using a Zeiss LSM800 confocal microscope and Zeiss Zen imaging software.
435
436 *Paraffin Sectioning and Hematoxylin & Eosin Staining*

437 Paraffin sectioning was performed by the Rutgers Cancer Institute of New Jersey Biospecimen Repository
438 and Histopathology Service Shared Resource. Decalcified juvenile fish were placed in 70% Ethanol.
439 Specimens were then dehydrated through a step protocol using ethanol and xylene and embedded in
440 paraffin using a Sakura Tissue-Tek VIP6 AI tissue processor and a Sakura Tissue-Tek TEC 6 tissue embedder.
441 Each mold was sectioned on a Leica Reichert-Jung BioCut 2030 rotary microtome at 4 μm. Slides were
442 then deparaffinized and stained with hematoxylin and eosin using a Sakura Tissue-Tek DRS 2000 slide
443 stainer.

444 *Statistical Analysis*
445 Data represent the mean ± SEM or are presented as scatter plots with the mean. All statistical analyses
446 were performed using GraphPad Prism v.8.20 (GraphPad, San Diego, CA). To compare *in vivo* data for two
447 groups, individual means were compared using the MannWhitney U test and Welch's t test. When
448 comparing more than three groups, normality was assessed using the Shapiro-Wilk test, then a two-way
449 ANOVA with Tukey's post hoc test was used for normally distributed samples or a Kruskal-Wallis test with
450 Dunn's post-hoc test was used for non-normally distributed samples. All statistical analyses were two-
451 sided tests, and p values of ≤ 0.05 were considered statistically significant.
452
453 **Acknowledgements**
454 The authors would like to thank Dr. James Dowling (Sick Kids, Toronto, ON, Canada) for donating the
455 sa146678 mutant line. We also thank Drs. John Dowling (Harvard University) and Ellen Townes-Anderson

(New Jersey Medical School) for helpful discussion on zebrafish photoreceptor phenotypes and retinal degeneration, and Dr. Matthew Alexander (University of Alabama, Birmingham) for discussion on the muscle phenotypes. We are particularly grateful to Kathleen Flaherty at the Rutgers Zebrafish Facility with assistance in the maintenance of the zebrafish colony and Lucyann Franciosa and Kelly Watkinswalton at the Rutgers Cancer Institute of New Jersey Biospecimen Repository and Histopathology Service Shared Resource for paraffin sectioning. The zn-8 developed by University of Oregon, Department of Neuroscience was obtained from the Developmental Studies Hybridoma Bank, created by the NICHD of the NIH and maintained at The University of Iowa, Department of Biology, Iowa City, IA 52242.

Conflict of Interest Statement. The authors declare no competing interests.

Funding

This work was funded by National Institute of Neurological Disorders and Stroke (R01NS109149 to M.C.M) and the Robert Wood Johnson Foundation (#74260 to M.C.M). B.F.K was supported by grant T32NS115700 from National Institute of Neurological Disorders and Stroke. Histopathology services in support of the research project were provided by the Rutgers Cancer Institute of New Jersey Biospecimen Repository and Histopathology Service Shared Resource supported in part with funding from National Cancer Institute (NCI-CCSG P30CA072720-5919).

Abbreviations

α-DS - α-dystroglycan

CMD - congenital muscular dystrophy

dpf – day post fertilization

ECM - extracellular matrix

Het – heterozygous

KO – knock-out

LGMD - limb-girdle muscular dystrophy

MO - morpholino oligonucleotides

OPL - outer plexiform layer

WT – wild type

WWS – Walker Warburg Syndrome

488 **References**

489 1. Bönnemann, C.G., Wang, C.H., Quijano-Roy, S., Deconinck, N., Bertini, E., Ferreiro, A., Muntoni, F.,
490 Sewry, C., Béroud, C., Mathews, K.D., *et al.* (2014) Diagnostic approach to the congenital muscular
491 dystrophies. Neuromuscular disorders : NMD, Vol. 24, pp. 289–311.

492 2. Kanagawa, M. (2021) Dystroglycanopathy: From Elucidation of Molecular and Pathological
493 Mechanisms to Development of Treatment Methods. *Int J Mol Sci*, 22, 13162.

494 3. Yoshida-Moriguchi, T. and Campbell, K.P. (2015) Matriglycan: a novel polysaccharide that links
495 dystroglycan to the basement membrane. *Glycobiology*, 25, 702–713.

496 4. Brancaccio, A. (2019) A molecular overview of the primary dystroglycanopathies. *J Cell Mol Med*, 23,
497 3058–3062.

498 5. Kim, D.-S., Hayashi, Y.K., Matsumoto, H., Ogawa, M., Noguchi, S., Murakami, N., Sakuta, R., Mochizuki,
499 M., Michele, D.E., Campbell, K.P., *et al.* (2004) POMT1 mutation results in defective glycosylation and
500 loss of laminin-binding activity in &agr;-DG. *Neurology*, 62, 1009–1011.

501 6. Graziano, A., Bianco, F., D'Amico, A., Moroni, I., Messina, S., Bruno, C., Pegoraro, E., Mora, M., Astrea,
502 G., Magri, F., *et al.* (2015) Prevalence of congenital muscular dystrophy in Italy: a population study.
503 *Neurology*, 84, 904–911.

504 7. Sframeli, M., Sarkozy, A., Bertoli, M., Astrea, G., Hudson, J., Scoto, M., Mein, R., Yau, M., Phadke, R.,
505 Feng, L., *et al.* (2017) Congenital muscular dystrophies in the UK population: Clinical and molecular
506 spectrum of a large cohort diagnosed over a 12-year period. *Neuromuscular Disord*, 27, 793–803.

507 8. Song, D., Dai, Y., Chen, X., Fu, X., Chang, X., Wang, N., Zhang, C., Yan, C., Zheng, H., Wu, L., *et al.* (2020)
508 Genetic Variations and Clinical Spectrum of Dystroglycanopathy in a Large Cohort of Chinese Patients.
509 *Clin Genet*.

510 9. Willer, T., Prados, B., Falcón-Pérez, J.M., Renner-Müller, I., Przemeck, G.K.H., Lommel, M., Coloma, A.,
511 Valero, M.C., Angelis, M.H. de, Tanner, W., *et al.* (2004) Targeted disruption of the Walker-Warburg
512 syndrome gene Pomt1 in mouse results in embryonic lethality. *Proceedings of the National Academy of*
513 *Sciences of the United States of America*, 101, 14126–14131.

514 10. Cohn, R.D., Henry, M.D., Michele, D.E., Barresi, R., Saito, F., Moore, S.A., Flanagan, J.D., Skwarchuk,
515 M.W., Robbins, M.E., Mendell, J.R., *et al.* (2002) Disruption of DAG1 in differentiated skeletal muscle
516 reveals a role for dystroglycan in muscle regeneration. *Cell*, 110, 639–648.

517 11. Satz, J.S., Barresi, R., Durbeej, M., Willer, T., Turner, A., Moore, S.A. and Campbell, K.P. (2008) Brain
518 and eye malformations resembling Walker-Warburg syndrome are recapitulated in mice by dystroglycan
519 deletion in the epiblast. *Journal of Neuroscience*, 28, 10567–10575.

520 12. Rubio-Fernández, M., Uribe, M.L., Vicente-Tejedor, J., Germain, F., Susín-Lara, C., Quereda, C.,
521 Montoliu, L., Villa, P. de la, Martín-Nieto, J. and Cruces, J. (2018) Impairment of photoreceptor ribbon

522 synapses in a novel Pomt1 conditional knockout mouse model of dystroglycanopathy. *Sci Rep-uk*, 8,
523 8543.

524 13. Li, M., Hromowyk, K.J., Amacher, S.L. and Currie, P.D. (2017) Chapter 14 Muscular dystrophy
525 modeling in zebrafish. *Methods Cell Biol*, 138, 347–380.

526 14. Widrick, J.J., Kawahara, G., Alexander, M.S., Beggs, A.H. and Kunkel, L.M. (2019) Discovery of Novel
527 Therapeutics for Muscular Dystrophies using Zebrafish Phenotypic Screens. *Journal of neuromuscular*
528 *diseases*, 6, 271–287.

529 15. Carss, K.J., Stevens, E., Foley, A.R., Cirak, S., Riemersma, M., Torelli, S., Hoischen, A., Willer, T.,
530 Scherpenzeel, M. van, Moore, S.A., *et al.* (2013) Mutations in GDP-Mannose Pyrophosphorylase B Cause
531 Congenital and Limb-Girdle Muscular Dystrophies Associated with Hypoglycosylation of α-Dystroglycan.
532 *American journal of human genetics*.

533 16. Stevens, E., Carss, K.J., Cirak, S., Foley, A.R., Torelli, S., Willer, T., Tambunan, D.E., Yau, S., Brodd, L.,
534 Sewry, C.A., *et al.* (2013) Mutations in B3GALNT2 Cause Congenital Muscular Dystrophy and
535 Hypoglycosylation of α-Dystroglycan. *American journal of human genetics*.

536 17. Manzini, M.C., Tambunan, D.E., Hill, R.S., Yu, T.W., Maynard, T.M., Heinzen, E.L., Shianna, K.V.,
537 Stevens, C.R., Partlow, J.N., Barry, B.J., *et al.* (2012) Exome sequencing and functional validation in
538 zebrafish identify GTDC2 mutations as a cause of Walker-Warburg syndrome. *American journal of*
539 *human genetics*, 91, 541–547.

540 18. Costanzo, S.D., Balasubramanian, A., Pond, H.L., Rozkalne, A., Pantaleoni, C., Saredi, S., Gupta, V.A.,
541 Sunu, C.M., Yu, T.W., Kang, P.B., *et al.* (2014) POMK mutations disrupt muscle development leading to a
542 spectrum of neuromuscular presentations. *Human Molecular Genetics*.

543 19. Avsar-Ban, E., Ishikawa, H., Manya, H., Watanabe, M., Akiyama, S., Miyake, H., Endo, T. and Tamaru,
544 Y. (2010) Protein O-mannosylation is necessary for normal embryonic development in zebrafish.
545 *Glycobiology*, 20, 1089–1102.

546 20. Gupta, V., Kawahara, G., Gundry, S.R., Chen, A.T., Lencer, W.I., Zhou, Y., Zon, L.I., Kunkel, L.M. and
547 Beggs, A.H. (2011) The zebrafish dag1 mutant: a novel genetic model for dystroglycanopathies. *Human*
548 *Molecular Genetics*, 20, 1712–1725.

549 21. Serafini, P.R., Feyder, M.J., Hightower, R.M., Garcia-Perez, D., Vieira, N.M., Lek, A., Gibbs, D.E.,
550 Moukha-Chafiq, O., Augelli-Szafran, C.E., Kawahara, G., *et al.* (2018) A limb-girdle muscular dystrophy 2I
551 model of muscular dystrophy identifies corrective drug compounds for dystroglycanopathies. *JCI insight*,
552 3, 199.

553 22. Liu, Y., Yu, M., Shang, X., Nguyen, M.H.H., Balakrishnan, S., Sager, R. and Hu, H. (2020) Eyes shut
554 homolog (EYS) interacts with matriglycan of O-mannosyl glycans whose deficiency results in EYS
555 mislocalization and degeneration of photoreceptors. *Sci Rep-uk*, 10, 7795.

556 23. Diesen, C., Saarinen, A., Pihko, H., Rosenlew, C., Cormand, B., Dobyns, W.B., Dieguez, J., Valanne, L.,
557 Joensuu, T. and Lehesjoki, A.-E. (2004) POMGnT1 mutation and phenotypic spectrum in muscle-eye-
558 brain disease. *Journal of Medical Genetics*, 41, e115.

559 24. Xu, M., Yamada, T., Sun, Z., Eblimit, A., Lopez, I., Wang, F., Manya, H., Xu, S., Zhao, L., Li, Y., *et al.*
560 (2016) Mutations in POMGNT1 cause non-syndromic retinitis pigmentosa. *Hum Mol Genet*, 25, 1479–
561 1488.

562 25. Abrams, E.W. and Mullins, M.C. (2009) Early zebrafish development: It's in the maternal genes. *Curr*
563 *Opin Genet Dev*, 19, 396–403.

564 26. Kettleborough, R.N.W., Busch-Nentwich, E.M., Harvey, S.A., Dooley, C.M., Bruijn, E. de, Eeden, F.
565 van, Sealy, I., White, R.J., Herd, C., Nijman, I.J., *et al.* (2013) A systematic genome-wide analysis of
566 zebrafish protein-coding gene function. *Nature*, 496, 494–497.

567 27. Manzini, M.C., Gleason, D., Chang, B.S., Hill, R.S., Barry, B.J., Partlow, J.N., Poduri, A., Currier, S.,
568 Galvin-Parton, P., Shapiro, L.R., *et al.* (2008) Ethnically diverse causes of Walker-Warburg syndrome
569 (WWS): FCMD mutations are a more common cause of WWS outside of the Middle East. *Human*
570 *Mutation*, 29, E231-41.

571 28. Godfrey, C., Clement, E., Mein, R., Brockington, M., Smith, J., Talim, B., Straub, V., Robb, S.,
572 Quinlivan, R., Feng, L., *et al.* (2007) Refining genotype phenotype correlations in muscular dystrophies
573 with defective glycosylation of dystroglycan. *Brain : a journal of neurology*, 130, 2725–2735.

574 29. Akasaka-Manya, K., Manya, H., Nakajima, A., Kawakita, M. and Endo, T. (2006) Physical and
575 functional association of human protein O-mannosyltransferases 1 and 2. *The Journal of biological*
576 *chemistry*, 281, 19339–19345.

577 30. Renninger, S.L., Gesemann, M. and Neuhauss, S.C.F. (2011) Cone arrestin confers cone vision of high
578 temporal resolution in zebrafish larvae. *Eur J Neurosci*, 33, 658–667.

579 31. Kohl, S., Baumann, B., Rosenberg, T., Kellner, U., Lorenz, B., Vadalà, M., Jacobson, S.G. and
580 Wissinger, B. (2002) Mutations in the Cone Photoreceptor G-Protein α-Subunit Gene GNAT2 in Patients
581 with Achromatopsia. *Am J Hum Genetics*, 71, 422–425.

582 32. Gao, P., Qin, Y., Qu, Z., Huang, Y., Liu, X., Li, J., Liu, F. and Liu, M. (2022) The Zpr-3 antibody
583 recognizes the 320-354 region of Rho and labels both rods and green cones in zebrafish. *Biorxiv*,
584 2022.02.21.481375.

585 33. El-Brolosy, M.A., Kontarakis, Z., Rossi, A., Kuenne, C., Günther, S., Fukuda, N., Kikhi, K., Boezio,
586 G.L.M., Takacs, C.M., Lai, S.-L., *et al.* (2019) Genetic compensation triggered by mutant mRNA
587 degradation. *Nature*, 568, 193–197.

588 34. Novak, J.S., Spathis, R., Dang, U.J., Fiorillo, A.A., Hindupur, R., Tully, C.B., Mázala, D.A.G., Canessa, E.,
589 Brown, K.J., Partridge, T.A., *et al.* (2021) Interrogation of Dystrophin and Dystroglycan Complex Protein
590 Turnover After Exon Skipping Therapy. *J Neuromuscul Dis*, 8, S383–S402.

591 35. Lindenmaier, L.B., Parmentier, N., Guo, C., Tissir, F. and Wright, K.M. (2019) Dystroglycan is a scaffold
592 for extracellular axon guidance decisions. *eLife*, 8, 239.

593 36. Clements, R. and Wright, K.M. (2018) Retinal ganglion cell axon sorting at the optic chiasm requires
594 dystroglycan. *Dev Biol*, 442, 210–219.

595 37. Wright, K.M., Lyon, K.A., Leung, H., Leahy, D.J., Ma, L. and Ginty, D.D. (2012) Dystroglycan organizes
596 axon guidance cue localization and axonal pathfinding. *Neuron*, 76, 931–944.

597 38. Davison, C. and Zolessi, F.R. (2021) Slit2 is necessary for optic axon organization in the zebrafish
598 ventral midline. *Cells Dev*, 166, 203677.

599 39. Novak, J.S., Spathis, R., Dang, U.J., Fiorillo, A.A., Hindupur, R., Tully, C.B., Mázala, D.A.G., Canessa, E.,
600 Brown, K.J., Partridge, T.A., *et al.* (2021) Interrogation of Dystrophin and Dystroglycan Complex Protein
601 Turnover After Exon Skipping Therapy. *J Neuromuscul Dis*, 8, S383–S402.

602 40. Sheikh, M.O., Capicciotti, C.J., Liu, L., Praissman, J., Ding, D., Mead, D.G., Brindley, M.A., Willer, T.,
603 Campbell, K.P., Moremen, K.W., *et al.* (2022) Cell surface glycan engineering reveals that matriglycan
604 alone can recapitulate dystroglycan binding and function. *Nat Commun*, 13, 3617.

605 41. Sato, S., Omori, Y., Katoh, K., Kondo, M., Kanagawa, M., Miyata, K., Funabiki, K., Koyasu, T., Kajimura,
606 N., Miyoshi, T., *et al.* (2008) Pikachurin, a dystroglycan ligand, is essential for photoreceptor ribbon
607 synapse formation. *Nature Neuroscience*, 11, 923–931.

608 42. Plump, A.S., Erskine, L., Sabatier, C., Brose, K., Epstein, C.J., Goodman, C.S., Mason, C.A. and Tessier-
609 Lavigne, M. (2002) Slit1 and Slit2 cooperate to prevent premature midline crossing of retinal axons in
610 the mouse visual system. *Neuron*, 33, 219–232.

611 43. Davison, C. and Zolessi, F.R. (2021) Slit2 is necessary for optic axon organization in the zebrafish
612 ventral midline. *Cells Dev*, 166, 203677.

613 44. Omori, Y., Araki, F., Chaya, T., Kajimura, N., Irie, S., Terada, K., Muranishi, Y., Tsujii, T., Ueno, S.,
614 Koyasu, T., *et al.* (2012) Presynaptic Dystroglycan-Pikachurin Complex Regulates the Proper Synaptic
615 Connection between Retinal Photoreceptor and Bipolar Cells. *J Neurosci*, 32, 6126–6137.

616 45. Clements, R., Turk, R., Campbell, K.P. and Wright, K.M. (2017) Dystroglycan Maintains Inner Limiting
617 Membrane Integrity to Coordinate Retinal Development. *Journal of Neuroscience*, 37, 8559–8574.

618 46. Kawahara, G., Gasperini, M.J., Myers, J.A., Widrick, J.J., Eran, A., Serafini, P.R., Alexander, M.S.,
619 Pletcher, M.T., Morris, C.A. and Kunkel, L.M. (2014) Dystrophic muscle improvement in zebrafish via
620 increased heme oxygenase signaling. *Human Molecular Genetics*, 23, 1869–1878.

621 47. Schindelin, J., Arg, I., Arganda-Carreras, I., a-Carreras, Frise, E., Kaynig, V., Longair, M., Pietzsch, T.,
622 Preibisch, S., Rueden, C., *et al.* (2012) Fiji: an open-source platform for biological-image analysis. 9, 676–
623 82.

624